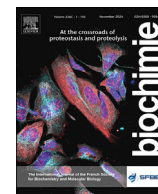




Contents lists available at ScienceDirect

Biochimie

journal homepage: www.elsevier.com/locate/biochi



Cathepsin D inhibition during neuronal differentiation selectively affects individual proteins instead of overall protein turnover

Johannes Schneider^{a, b}, Julia Mitschke^{a, c, d}, Mahima Bhat^{a, e}, Daniel Vogele^{e, f},
Oliver Schilling^{c, d, f, g}, Thomas Reinheckel^{a, c, d, g, *}, Lisa Heß^a

^a Institute of Molecular Medicine and Cell Research, Faculty of Medicine, University of Freiburg, 79104, Freiburg, Germany

^b Faculty of Medicine, University of Freiburg, 79104, Freiburg, Germany

^c German Cancer Consortium (DKTK), partner site Freiburg, 79104, Freiburg, Germany

^d German Cancer Research Center (DKFZ), 69120, Heidelberg, Germany

^e Faculty of Biology, University of Freiburg, 79104, Freiburg, Germany

^f Institute for Surgical Pathology, Medical Center - University of Freiburg, Faculty of Medicine, University of Freiburg, 79104, Freiburg, Germany

^g Centre for Biological Signalling Studies BIOSS, University of Freiburg, 79104, Freiburg, Germany

ARTICLE INFO

Article history:

Received 20 December 2023

Received in revised form

6 March 2024

Accepted 22 March 2024

Available online 28 March 2024

Handling Editor: Dr B Friguet

Keywords:

Cathepsin D

Neurodegeneration

LUHMES cell line

Proteolysis

ABSTRACT

Cathepsin D (CTSD) is a lysosomal aspartic protease and its inherited deficiency causes a severe pediatric neurodegenerative disease called neuronal ceroid lipofuscinosis (NCL) type 10. The lysosomal dysfunction in the affected patients leads to accumulation of undigested lysosomal cargo especially in non-dividing cells, such as neurons, resulting in death shortly after birth. To explore which proteins are mainly affected by the lysosomal dysfunction due to CTSD deficiency, Lund human mesencephalic (LUHMES) cells, capable of inducible dopaminergic neuronal differentiation, were treated with Pepstatin A. This inhibitor of “acidic” aspartic proteases caused accumulation of acidic intracellular vesicles in differentiating LUHMES cells. Pulse-chase experiments involving stable isotope labelling with amino acids in cell culture (SILAC) with subsequent mass-spectrometric protein identification and quantification were performed. By this approach, we studied the degradation and synthesis rates of 695 and 680 proteins during early and late neuronal LUHMES differentiation, respectively. Interestingly, lysosomal bulk proteolysis was not altered upon Pepstatin A treatment. Instead, the protease inhibitor selectively changed the turnover of individual proteins. Especially proteins belonging to the mitochondrial energy supply system were differentially degraded during early and late neuronal differentiation indicating a high energy demand as well as stress level in LUHMES cells treated with Pepstatin A.

© 2024 The Author(s). Published by Elsevier B.V. This is an open access article under the CC BY-NC-ND license (<http://creativecommons.org/licenses/by-nc-nd/4.0/>).

1. Introduction

Proteolysis is central for the homeostasis as well as survival of neurons and therefore, for a proper function of the brain itself [1]. Aberrant states of certain proteins cause a variety of neurodegenerative disorders like Alzheimer's (AD), Huntington's (HD) or Parkinson's disease (PD). All of these neurodegenerative disorders accumulate protein aggregates, which cannot be cleared from the brain. Another group of neurodegenerative disorders is caused by lysosomal dysfunction and called lysosomal storage diseases (LSDs) [2,3]. These LSDs accumulate undigested material within lysosomes

mainly due to impaired function of lysosomal hydrolases. The clinical severity of LSDs depends on the degree of lysosomal dysfunction ranging from mild retardation to death within hours after birth.

The most common group of pediatric neurodegenerative diseases in humans belonging to those LSDs are the neuronal ceroid lipofuscinoses (NCLs) [4]. Those mainly recessively inherited NCLs are categorized by the affected gene into at least 14 different subtypes [4,5]. NCL type 10 is caused by a number of different loss-of-function mutations in the human cathepsin D (CTSD) gene [6,7]. Notably, NCL type 10 represents one of the severe congenital NCL subtypes, most often resulting in death of the patients shortly after birth. CTSD belongs to the small group of aspartic proteases together with cathepsin E (CTSE) and pepsinogen mainly present in the gut [2]. In contrast to gastric pepsin, CTSD and CTSE are

* Corresponding author. Institute of Molecular Medicine and Cell Research, Faculty of Medicine, University of Freiburg, 79104 Freiburg, Germany.

E-mail address: thomas.reinheckel@mol-med.uni-freiburg.de (T. Reinheckel).

proteases catalyzing the hydrolysis of proteins in the acidic endo-lysosomal compartment [8]. Mice with a constitutive deficiency of CTSD present with NCL symptoms about three weeks after birth and die on postnatal day 26 ± 1 [9]. Histological analysis of brains of those mice revealed a substantial loss of neurons accompanied by strong proliferation and activation of microglia and astroglia cells (gliosis) [10,11]. Furthermore, CTSD-deficient mice presented with an atrophy of their thymus as well as small intestine contributing to the early death of mice [11,12]. CTSD deficiency restricted to the neuroectoderm (mainly neurons) of mice showed only a slightly delayed NCL phenotype compared to a constitutive CTSD deficiency with neuronal loss accompanied by gliosis, atrophy of thymus as well as small intestine and death on postnatal day 31.5 [11]. These results demonstrate that the lysosomal dysfunction in neurons seem to be the main driver of NCL type 10.

Therapeutic options for patients with NCL are very limited [13]. At the moment, enzyme replacement therapy (ERT) seems to improve the outcome of patients with NCL. The only approved ERT for NCL is the intraventricular administration of recombinant tripeptidyl-peptidase 1 (TPP1) for patients with NCL type 2 [14]. That this strategy may also work for patients suffering from NCL type 10 was shown by administering recombinant human CTSD intracranial to constitutive CTSD-deficient mice, thereby reducing the lysosomal storage phenotype in the brain and delaying the neuropathological phenotype of CTSD-deficient mice compared to untreated controls [13].

Although this therapeutic approach seems to be very promising in restoring lysosomal function, generating more knowledge about how CTSD affects proteolysis may offer new strategies to treat NCL type 10. Therefore, our study focused on how CTSD inhibition may affect protein turnover in a human neuronal differentiation model. For that purpose, Lund human mesencephalic (LUHMES) cells [15] were treated with Pepstatin A (PepA), an inhibitor of acidic aspartic proteases (CTSD/CTSE), and protein turnover during early and late neuronal differentiation was analyzed using stable isotope labelling with amino acids in cell culture (SILAC). This analysis demonstrated that individual proteins were stabilized or destabilized upon Pepstatin A administration instead of having an effect on overall lysosomal proteolysis. Furthermore, this seems to be a very dynamic process, because a remarkable difference in the proteins being stabilized or destabilized upon Pepstatin A treatment was revealed between early and late neuronal differentiation of LUHMES cells.

2. Materials and methods

2.1. Cell culture and treatments

LUHMES cells were cultured as previously described [15]. Shortly, Nunc™ flasks or well plates were coated with 1 mg/ml Poly-L-Ornithine (Sigma-Aldrich) at 37 °C overnight, washed once with sterile ddH₂O and air-dried in aseptic conditions. Proliferation medium (1x N-2 Supplement, 2 mM L-glutamine, 40 ng/ml recombinant human fibroblast growth factor (rhFGF) in advanced DMEM/F-12) was used to culture the proliferating precursor LUHMES cells and differentiation was induced by differentiation medium (1x N-2 Supplement, 2 mM L-glutamine, 1 mM cyclic adenosine monophosphate (cAMP), 2 ng/ml recombinant human glial cell line-derived neurotrophic factor (rhGDNF), 1 µg/ml Tetracycline in advanced DMEM/F-12). To inhibit aspartic proteases (CTSD/E), cells were treated with 15 µM Pepstatin A or solvent DMSO.

2.2. qRT-PCR

RNA isolation and qRT-PCR was done as previously described [16]. Shortly, cells were harvested and lysed using the Total RNA Kit (peqGold). RNA was transcribed to cDNA using the iScript™ cDNA Synthesis Kit (Bio-Rad). Transcribed cDNA was diluted, mixed with SYBR™ Select Master Mix (Thermo Fisher Scientific) as well as forward and reverse primers of Table 1 and finally measured in the Real-Time PCR Detection System (Bio-Rad). Average of technical replicates was normalized to GAPDH using the $\Delta\Delta C_t$ method.

2.3. Aspartic protease activity assay

Aspartic protease activity assay was performed as previously described [16]. Shortly, cells were harvested and resuspended in sodium acetate buffer (100 mM sodium acetate, 1 mM EDTA, 0.05% Brij 35, and 1 mM DTT in H₂O, pH 4.0) and homogenized using the Bioruptor sonication device (Diagenode). 25 µM of the fluorogenic substrate Mca-Gly-Lys-Pro-Ile-Leu-Phe-Phe-Arg-Leu-Lys(Dnp)-D-Arg-NH₂ (Bachem, M – 2455) was mixed with the cell lysates of similar protein concentration and measured every minute for 1 h at 393 nm (excitation at 328 nm) using the EnSpire multimode plate reader (PerkinElmer).

2.4. LysoTracker™ staining

LysoTracker™ staining was done as described previously [17]. Shortly, cells were detached, washed twice with DPBS and resuspended in FACS buffer (2% FCS, 5 mM EDTA in DPBS). Cells were stained with LysoTracker™ Green DND-26 (1:10000; Thermo Fisher Scientific) at 37 °C and 5% CO₂ for 15 min, measured with the CytoFLEX S (Beckman Coulter) and analyzed with FlowJo software (BD Biosciences).

2.5. Stable isotope labelling with amino acids in cell culture (SILAC) pulse-chase

For the SILAC experiment, LUHMES cells were cultured in medium containing medium-labelled Lysine (¹³C₆) and Arginine (¹³C₆) for at least 5 replication cycles. Two days prior starting neuronal differentiation of LUHMES cells, 15 µM Pepstatin A or its solvent DMSO was added to the medium. To detect protein turnover during early differentiation, the change to differentiation medium was simultaneous with the exchange of medium-labelled amino acids by heavy-labelled amino acids (pulse; Lys¹³C₆,¹⁵N₂; Arg¹³C₆,¹⁵N₄). For the investigation of protein turnover during late neuronal differentiation, the described pulse was done starting on day 4 of differentiation. Samples for protein isolation were obtained 0 h, 12 h, 24 h and 48 h after each pulse (chase). Here, cells were washed once with DPBS and harvested in DPBS by a cell scraper and transferred in an Eppendorf tube followed by centrifugation at

Table 1
Sequence of forward and reverse primers used for qRT-PCR.

Target	Primer forward (5'-3')	Primer reverse (5'-3')
CTSD	ATTCCCGAGGTGCTCAAGAA	AAGCGATGTCACGAGTTTG
CTSE	ACTAGCCAGCCTGCAAGAC	GGCCAACACGGTTAGTCCTT
GAPDH	CGACCACTTTGTCAAGCTCA	AGGGGTCTACATGGCAACTG
KCNJ6	TGGCCAAGCTGACAGAATCCA	CCTGGCTGCTTAGGCAACT
NRG1	TGTGCAAGTGCCAACCTGGATT	GGCGATGCAGATGCCGGTTA
SOX2	GAAGGATAAGTACACGCTGCCCG	GCTGGTCATGGAGTTGTACTGC
Syn1	TCAGACCTTCTACCCCAATCA	GTCTGGAAGTCATGCTGGT

300g for 5 min to generate a cell pellet.

2.6. Protein isolation

Proteins were isolated from cell pellets obtained from the above described SILAC pulse-chase experiment as described previously [18] using micro S-TRAP columns (PROTIFY) according to the manufacturer's protocol [19]. Shortly, cell pellets were lysed in SDS lysis buffer (5% SDS, 50 mM triethylammonium bicarbonate (TEAB), pH 7.55) and sonicated for 1 s using a sample sonicator at 50% amplitude (Branson W-450 D) followed by reduction and alkylation with 5 mM tris(2-carboxyethyl)phosphine hydrochloride (TCEP) at 95 °C for 10 min and 20 mM chloroacetamide (CAA) at 37 °C for 30 min in the dark. A maximum of 100 µg protein diluted in loading buffer (100 mM TEAB in 90% methanol, pH 7.1) was acidified with phosphoric acid and transferred on a column followed by washing four times with loading buffer. Proteins were digested with 1 µg/20 µg protein trypsin in 50 mM TEAB (pH 8) at 47 °C for 1 h. Elution of generated peptides was done in three successive steps using first 50 mM TEAB (pH 8), then 0.2% formic acid and last 50% acetonitrile with 0.2% formic acid. Peptide concentration was measured and 5 µg of each sample was vacuum-dried and stored at –80 °C until mass spectrometric measurement.

2.7. Mass spectrometry (MS)

For MS measurement, vacuum dried peptides were resolubilized in 0.1% (v/v) formic acid, sonicated for 5 min and centrifuged at 20000 g for 10 min before transferring the supernatant to a measurement tube. 800 ng of each sample, together with 200 fmol of indexed retention time (iRT) peptides, were analyzed using a nanoflow liquid chromatography (LC) system Easy-nLC 1000 (Thermo Fisher Scientific) equipped with a trapping column (Acclaim™ PepMap™ 100) and an analytical column (200 cm micro pillar array columns (µPAC™), Thermo Fisher Scientific) tempered to 45 °C. Samples were trapped at 200 bars with 100% buffer A (0.1% v/v formic acid) and separated using a dynamic flow rate of 350–700 nL/min. A 120 min multistep gradient of 8%–55% buffer B (80% v/v acetonitrile, 0.1% v/v formic acid) in buffer A was used for separation, followed by washing (100% buffer B) and reconditioning of the column to 8% buffer B. The Easy-nLC 1000 system was coupled online to a Q-Exactive plus mass spectrometer (Thermo Fisher Scientific) via a Nanospray Flex IonSource (Thermo Fisher Scientific) with an applied voltage of 2.1 kV for electrospray ionization. The analytical column was coupled to a pulled, uncoated Electrospray Ionization (ESI) emitter (10 µm tip inner diameter, 20 µm inner diameter, 7 cm length, CoAnn Technologies) via a µPac™ Flex iON Connect ESI-MS interface (PharmaFluidics). The mass spectrometer was operated in data dependent acquisition mode and each MS scan was followed by a maximum of 16 MS/MS scans (Top16 method). The mass range from 300 to 2000 *m/z* (mass-to-charge ratio) was analyzed. MS1 resolution was set to 70000, automatic gain control (AGC) to 3e6 and maximum injection time was set to 50 ms. MS2 resolution was set to 17500, AGC to 1e5 and maximum injection time to 80 ms using stepped normalized collision energy (NCE) of 25 and 30 for fragmentation.

2.8. Western blot

Protein isolation, SDS-PAGE and wetblot were done as previously described [16]. For immunoblotting, the nitrocellulose membranes were incubated with 3% BSA in PBS for 1 h followed by incubation with primary antibodies of Table 2 overnight. After

Table 2

Primary and secondary antibodies used for Western blot.

Target	Company	Dilution
CYC1	Invitrogen, PA5-51550	1:500
NDUFS3	Abcam, ab183733	1:500
SUPV3L1	Proteintech, 12826-1-AP	1:500
TUBA	Sigma-Aldrich, T9026	1:1000
IRDye® 800CW Donkey anti-Mouse IgG	LI-COR, 926-32212	1:10000
IRDye® 680RD Donkey anti-Rabbit IgG	LI-COR, 926-68073	1:10000

washing the membranes with PBST, secondary antibody was applied for 1 h followed by washing. The membranes were analyzed using the Odyssey DLx (LI-COR) and Image Studio Lite software (LI-COR).

2.9. Data analysis, presentation and statistics

Data obtained from qRT-PCR, aspartic protease activity assay and Lysotracker™ staining were visualized in line or bar charts expressed as mean ± SEM or mean + SEM, respectively. For Western blot data, individual data points connected to the different conditions of the corresponding biological replicate were shown. *n* represents independent experiments. These statistical analyses were done with OriginPro 2020 (OriginLab) with comparison of two groups by two-sided one-sample *t*-test, two-sided paired-sample *t*-test or one-way ANOVA.

Raw data obtained from the SILAC-based mass spectrometry was analyzed using FragPipe pipeline (v17.1) [20–22] with a human proteome database containing Uniprot sequences downloaded from Uniprot on 05th May 2022 (21149 entries). Decoys for the database search were generated using the implemented function in the FragPipe database section. A precursor mass tolerance of 10/10 ppm and fragment mass tolerance of 20 ppm was used. Tryptic cleavage specificity with two missed cleavages was applied. Carbamidomethyl at cysteines was the only fixed modification, whereas protein N-terminal and lysine acetylation was set as variable modification with mass deltas corresponding to medium (42.0106 Da) and heavy (46.03263 Da) isotopic labels. Quantification was performed on MS1 level using the IonQuant, accounting for the medium and heavy mass deltas introduced by SILAC labeling. Further analysis of the generated peptide list was performed with R Space and visualized by OriginPro 2020 (relative fractional labeling, venn diagram and heat maps) or the R package *tidyverse* including *ggplot* [23] (change of protein stability; R-Scripts are provided upon request by the corresponding author). The identified stabilized or destabilized proteins upon Pepstatin A treatment for each condition were clustered using the Search Tool for the Retrieval of Interacting Genes/Proteins (STRING) [24].

3. Results

3.1. Cathepsin D inhibition induces accumulation of acidic vesicles in LUHMES cells

LUHMES cells are neuronal precursors, which were transfected with a Tetracycline (Tet)-off system expressing *v-myc* for constant proliferation [15,25]. Upon Tetracycline treatment, expression of *v-myc* is abrogated resulting in stop of proliferation and subsequent homogeneous differentiation of LUHMES cells into mature dopaminergic neurons after 5–6 days. During this process, the cells establish a neuronal network by the formation of neurites (Fig. 1A). We validated the differentiation status of LUHMES cells by examination of proliferation and neuronal differentiation markers. In

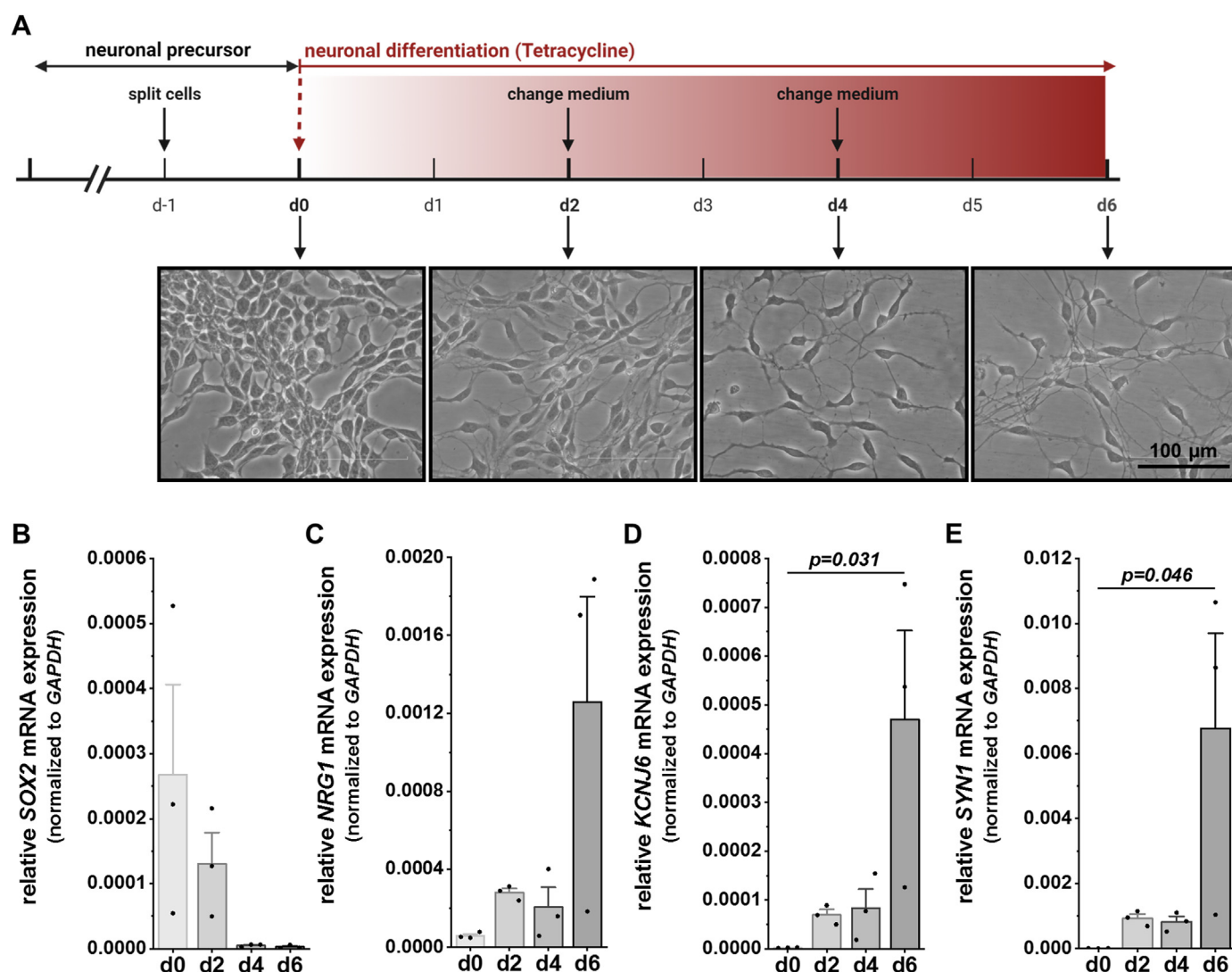


Fig. 1. Neuronal differentiation of LUHMES cells. (A) Outline of neuronal differentiation of LUHMES cells with microscopy pictures on indicated time points during differentiation. LUHMES cells were treated with Tetracycline and became mature after 5–6 days of differentiation (outline created with [BioRender.com](#)). (B–E) Relative mRNA expression of SOX2 (B), *NRG1* (C), *KCNJ6* (D) and *SYN1* (E) on day 0, 2, 4 and 6 of neuronal differentiation of LUHMES cells measured by qRT-PCR ($n = 3$ independent experiments; One-way ANOVA). Bar charts show all data points with mean \pm SEM and p -values.

LUHMES cells, expression of the proliferation marker sex-determining region (SRY)-box 2 (*SOX2*; Fig. 1B) was reduced, whereas expression of the neuronal differentiation markers *neuregulin 1* (*NRG1*; Fig. 1C), G protein-activated inward rectifier potassium channel 2 (*KCNJ6*; Fig. 1D) as well as *synapsin 1* (*SYN1*; Fig. 1E) was upregulated upon neuronal differentiation induced by tetracycline.

After demonstrating successful neuronal differentiation of the *in vitro* model, we treated LUHMES cells with Pepstatin A (PepA) inhibiting aspartic proteases (CTSD/CTSE) to model CTSD deficiency that occurs in patients with NCL type 10 (Fig. 2A). The efficacy of Pepstatin A was determined in an enzyme activity assay showing a decrease in aspartic protease activity upon Pepstatin A treatment with a concentration of 15 μ M (Fig. 2B). Notably, *CTSE* mRNA was not expressed in LUHMES cells, which was confirmed by detectable *CTSE* levels in a human hepatocellular carcinoma cell line (Huh-7) and colorectal cancer cell line (LoVo) expressing CTSE according to The Human Protein Atlas ([proteintlas.org](#); [26]) (Fig. 2C). In

contrast, for *CTSD* high mRNA expression with slight upregulation upon neuronal differentiation was measured in LUHMES cells (Fig. 2D). Due to the absence of *CTSE* mRNA expression, it is evident that CTSE is not present in LUHMES cells and the inhibitory effect of Pepstatin A is affecting CTSD rather than CTSE activity.

A hallmark of NCL remains the accumulation of lysosomes and their engulfed material in cells. To test whether Pepstatin A treatment during neuronal differentiation of LUHMES cells results in a similar phenotype, LUHMES cells were stained with LysoTracker™ Green DND-26 to visualize the acidic compartment and quantified by flow cytometry. Control cells were treated with the same amount of DMSO used as solvent for Pepstatin A. The acidic compartment was significantly increased upon use of Pepstatin A during neuronal differentiation of LUHMES cells (Fig. 2E). Therefore, treatment of human LUHMES cells with Pepstatin A during neuronal differentiation seems to be a suitable *in vitro* model for biochemical and molecular studies on NCL type 10.

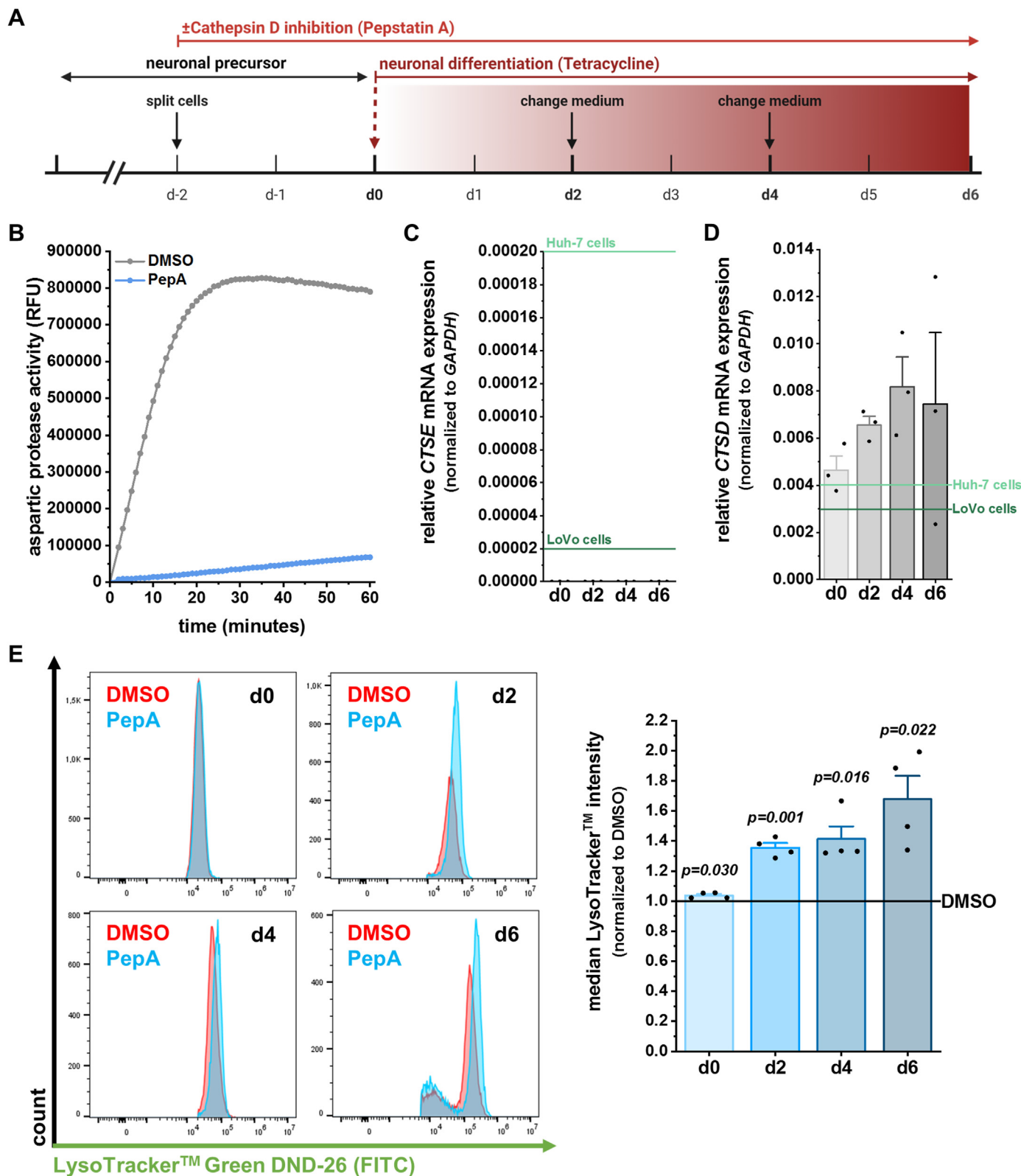


Fig. 2. Treatment of LUHMES cells with Pepstatin A during neuronal differentiation. (A) Outline of neuronal differentiation of LUHMES cells and treatment with Pepstatin A (created with BioRender.com). (B) Aspartic protease activity in LUHMES cells \pm 15 μ M Pepstatin A treatment ($n = 1$ independent experiment). (C–D) Relative mRNA expression of *CTSE* (C) and *CTSD* (D) on day 0, 2, 4 and 6 of neuronal differentiation of LUHMES cells measured by qRT-PCR ($n = 3$ independent experiments). Expression levels in LUHMES cells were compared to Huh-7 cells (light green; $n = 1$ independent experiment) and LoVo cells (dark green; $n = 1$ independent experiment). (E) Flow cytometry analysis of LysoTracker™ Green DND-26 staining of LUHMES cells \pm 15 μ M Pepstatin A on day 0, 2, 4 and 6 of neuronal differentiation ($n = 3$ independent experiments, two-sided one-sample t -test). Line charts show the mean \pm SEM, bar charts show all data points with mean \pm SEM and p -value.

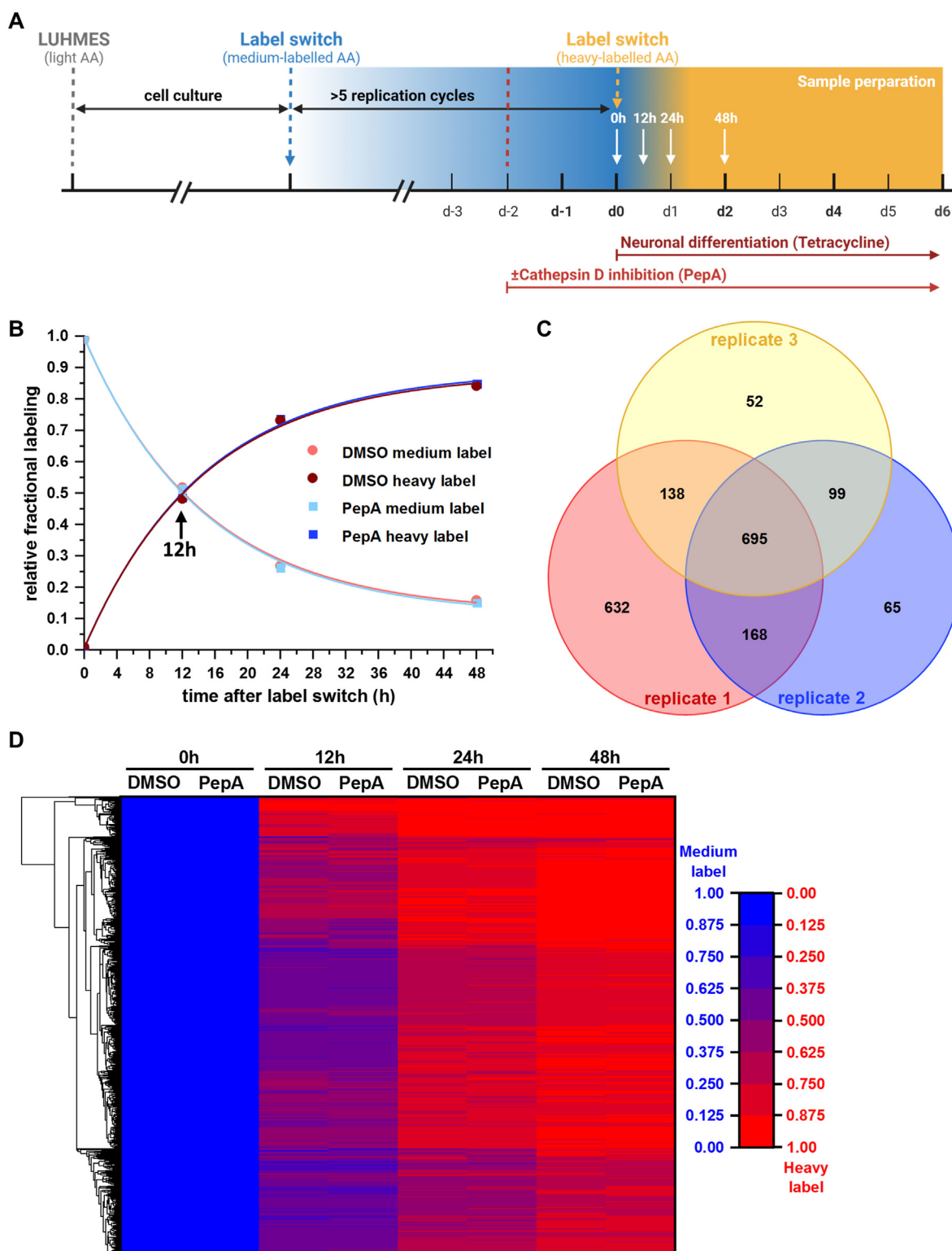


Fig. 3. Protein turnover in LUHMES cells treated with Pepstatin A during early neuronal differentiation. (A) Outline of neuronal differentiation of LUHMES cells, treatment with 15 μ M Pepstatin A and label switches (created with [BioRender.com](https://www.biorender.com)). (B) Change of relative fractional labelling for medium (light red: DMSO; light blue: PepA) and heavy label (dark red: DMSO; dark blue: PepA) in LUHMES cells \pm 15 μ M Pepstatin A at 0 h, 12 h, 24 h and 48 h after switch to heavy label during early neuronal differentiation. (C) Venn diagram showing detected proteins in three independent biological replicates of LUHMES cells used for SILAC experiment during early neuronal differentiation. (D) Heat map of protein decay in LUHMES cells \pm 15 μ M Pepstatin A at 0 h, 12 h, 24 h, and 48 h after switch to heavy label during early neuronal differentiation. (n = 3 independent experiments).

3.2. Cathepsin D inhibition during early neuronal differentiation does not affect bulk protein turnover in LUHMES cells

We used a pulse-chase variant of SILAC to determine the protein turnover upon Pepstatin A treatment during early differentiation of LUHMES cells. First, Lys¹³C₆ and Arg¹³C₆ isotopes replaced the Lys¹²C₆ and Arg¹²C₆ in the cell culture medium, thereby labeling all proteins with the ¹³C₆ amino acids. This state will be further annotated as “medium label” (Fig. 3A). After five cell divisions, treatment with Pepstatin A started two days prior to induction of neuronal differentiation. To determine protein turnover during early neuronal differentiation, isotope label switch accompanied induction of neuronal differentiation. For this, the medium containing Lys¹³C₆ and Arg¹³C₆ was changed for medium containing the “heavy” amino acids Lys¹³C₆,¹⁵N₂ and Arg¹³C₆,¹⁵N₄. Cellular proteins were isolated immediately at label switch (0 h) as well as 12 h, 24 h and 48 h after label switch. Subsequently, the proteins were converted to tryptic peptides and analyzed by LC-MS/MS mass spectrometry.

As expected, medium-labelled proteins declined, whereas heavy-labelled proteins increased after the last label switch (Fig. 3B). Equilibrium of medium and heavy labels was reached at about 12 h after label switch. Interestingly, Pepstatin A treatment caused no difference in general protein turnover as its curves strongly overlap with the control condition. For further analysis, only proteins present in all three independent biological replicates (695 proteins) were included (Fig. 3C). To investigate the protein decay, the ratio of medium-labelled (ML) to medium- and heavy-labelled (HL) proteins for each time point (t) was calculated using formula 1.

$$\text{protein decay} = \frac{\text{intensity ML protein (t)}}{\text{intensity ML protein (t)} + \text{intensity HL protein (t)}} \quad (1)$$

Protein decay was visualized by a heat map showing a reduction of medium-labelled proteins (blue to red) during neuronal differentiation as already indicated above (Fig. 3D). However, some proteins demonstrated a difference in decay as a result of treatment with Pepstatin A indicating selectively dysregulated proteolysis of individual proteins.

3.3. Cathepsin D inhibition during early neuronal differentiation increases the stability of proteins of the electron transport chain and neurite outgrowth in LUHMES cells

Changes of protein stability upon Pepstatin A treatment during early neuronal differentiation was measured using formula 2 and again visualized in a heat map (Fig. 4A). A change of the color to red indicated a stabilization, whereas a shift to green indicated destabilization of the respective protein upon Pepstatin A treatment.

$$\text{protein stability} = \frac{\text{protein turnover PepA (t)}}{\text{protein turnover DMSO (t)}} \quad (2)$$

To identify the most stable as well as unstable proteins, the mean of the protein stability at 12, 24 and 48 h of early neuronal differentiation was calculated for each protein and all proteins with a value higher or lower than $\pm 1x$ standard deviation (SD) were categorized as stabilized or destabilized proteins upon Pepstatin A treatment, respectively (Fig. 4B). In total, we identified 77 stabilized proteins (red; Supplementary Table S1) and 74 destabilized proteins (blue; Supplementary Table S2) and subjected them to STRING

analysis (stabilized proteins: Supplementary Fig. S1A; destabilized proteins: Supplementary Fig. S1B). Analysis of the formed clusters revealed clusters of affected proteins in mitochondria as well as in the cytoskeleton (Fig. 4C). In mitochondria, proteins important for the electron transport chain stabilized upon Pepstatin A treatment, whereas proteins degrading mitochondrial mRNA were destabilized. General changes in the cytoskeleton were expected due to its extensive rearrangement upon neuronal differentiation [27]. Nevertheless, Pepstatin A treatment increased the stability of proteins important for neurite outgrowth and reduced the stability of proteins maintaining actin cross-links as well as actin filaments compared to control conditions. These results indicate a higher energy demand and stronger efforts to build up a neuronal network in LUHMES cells treated with Pepstatin A compared to controls.

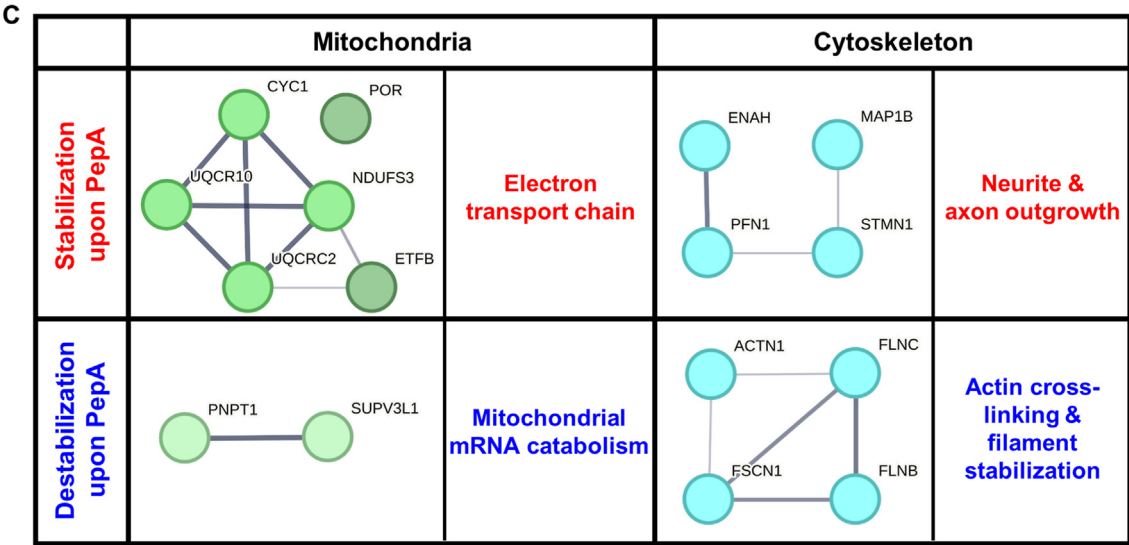
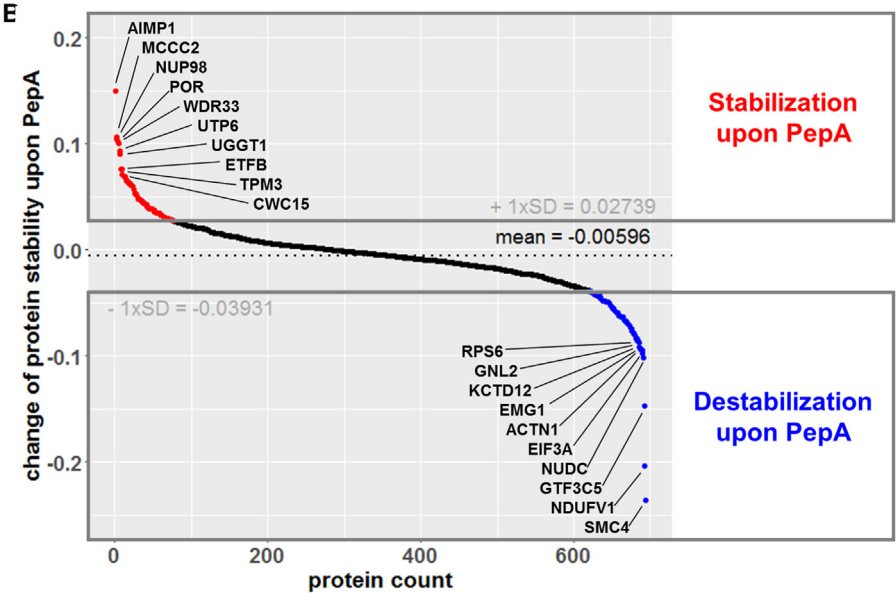
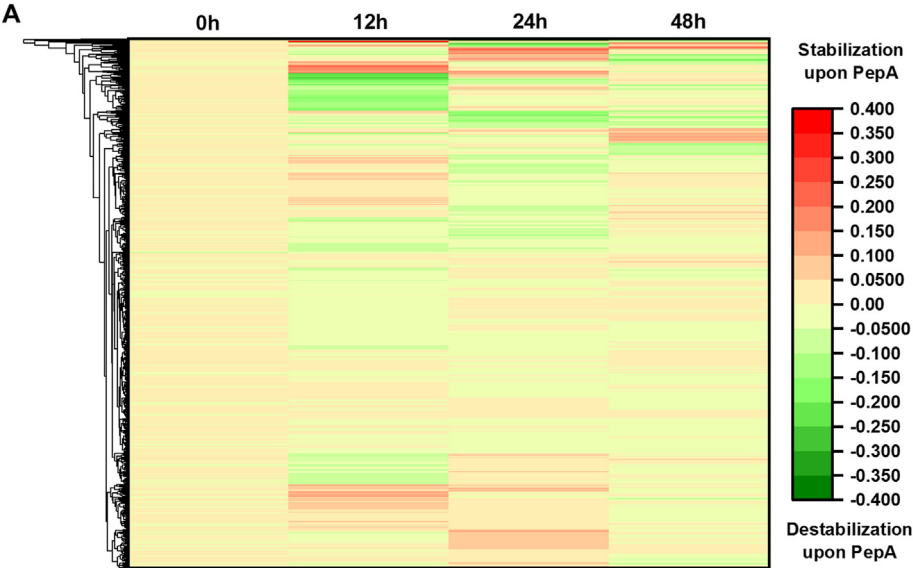
3.4. Cathepsin D inhibition during late neuronal differentiation does not affect bulk protein turnover in LUHMES cells

To detect protein turnover at later stages of neuronal differentiation, we modified the pulse-chase SILAC approach to a label switch after four days of differentiation (Fig. 5A). As in the early differentiation experiments, the medium-labelled proteins declined, while the heavy label increased over time with no effect of Pepstatin A treatment on general protein turnover (Fig. 5B). However, the loss of Lys¹³C₆ and Arg¹³C₆ peptides and the corresponding gain of heavy label was slower in late differentiation with label equilibrium at about 32 h after label switch compared to 12 h during early differentiation. In total 680 proteins were detected in three independent biological replicates, which were used for further analysis (Fig. 5C). Protein decay was calculated according to formula 1 and visualized using a heat map (Fig. 5D). The heat map also shows the generally slower protein decay during late differentiation, as most proteins identified after 12 h remained blue and turn mainly red 48 h after the label change. Nevertheless, we also found differences in protein decay of individual proteins upon Pepstatin A treatment during late neuronal differentiation.

3.5. Cathepsin D inhibition during late neuronal differentiation affects mitochondrial energy production and increases the stability of proteins of the vesicular transport system in LUHMES cells

Again, protein stability was calculated according to formula 2 and shown in a heat map demonstrating how individual proteins change as a result of Pepstatin A treatment (Fig. 6A). The data of all identified proteins were examined for stabilized or destabilized proteins (Fig. 6B). These analyses yielded 72 stabilized (red; Supplementary Table S3) and 73 destabilized proteins (blue; Supplementary Table S4), which were used for further exploration by the STRING algorithms (stabilized proteins: Supplementary Fig. S2A; destabilized proteins: Supplementary Fig. S2B). The STRING analysis revealed an interesting phenomenon in mitochondria (Fig. 6C). During early neuronal differentiation proteins belonging to the electron transport chain were stabilized, however during late differentiation, this class of proteins was destabilized, while proteins responsible for fatty acid oxidation and antioxidative actions were stabilized upon Pepstatin A treatment.

We validated these results by analyzing the protein levels of NDUFS3 stabilized and SUPV3L1 destabilized during early differentiation due to the use of Pepstatin A in the SILAC turnover study (Fig. 4C). In fully differentiated LUHMES cells NDUFS3 (Supplementary Fig. S3A) levels showed a tendency to be increased, whereas SUPV3L1 (Supplementary Fig. S3B) expression was reduced upon Pepstatin A treatment. Additionally, we analyzed the



protein levels of CYC1, which was stabilized during early differentiation (Fig. 4C), but destabilized during late differentiation (Fig. 6C) upon treatment with Pepstatin A in the SILAC turnover experiments. A tendency to decreased protein expression was measured in mature LUHMES cells upon Pepstatin A treatment (Supplementary Fig. S3C), which is in line with the results of the SILAC experiments performed during late neuronal differentiation.

In total 15 proteins were identified which were initially stabilized during early and destabilized during late neuronal differentiation upon Pepstatin A treatment or vice versa (Supplementary Table S5). Only two proteins each remained stable or unstable due to the use of Pepstatin A during early as well as late neuronal differentiation. Furthermore, we measured an expected increase in the stability of proteins belonging to the vesicular transport system. Especially the higher stability of the lysosomal proteins LAMP1 and SCARB2 indicates that the observed lysosomal storage phenotype in NCL patients develops during late differentiation of neurons, because no lysosomal proteins were found stabilized and LAMP1 was even destabilized during early neuronal differentiation (Supplementary Fig. S1A; Supplementary Table S5). Analysis of LAMP1 protein levels in proliferating (d0), early differentiated (d2) and late differentiated (d6) LUHMES cells verified the increased stability in Pepstatin A-treated mature neurons compared to controls, whereas no change of LAMP1 levels was measured in precursors and immature neurons (Supplementary Fig. S3D). High LAMP1 protein levels due to a loss of function of CTSD seem to persist shown by analysis of a whole brain lysate of a *Ctsd*-deficient mouse compared to a control mouse (Supplementary Fig. S3E).

Interestingly, only three other proteases were identified to be differentially stabilized upon Pepstatin A treatment during late neuronal differentiation, all being involved in the Ubiquitin-Proteasome System (UPS) (Supplementary Fig. S3F). The ubiquitin carboxyl-terminal hydrolase 7 (USP7), a deubiquitinating enzyme [28], was stabilized upon Pepstatin A treatment. In contrast, the proteasome subunit alpha type 2 (PSMA2), a proteolytic component of the 20S core proteasome complex [29], and tripeptidyl-peptidase 2 (TPP2), a N-terminal tripeptidase acting downstream of the proteasome [30], were destabilized due to the use of Pepstatin A. This indicates that both major protein degradation pathways, autophagy using lysosomes as well as the UPS, are dysregulated due to Pepstatin A treatment during late neuronal differentiation of LUHMES cells.

4. Discussion

Cathepsin D is the most abundant lysosomal protease [1,31]. It is central for the homeostasis of neurons as impaired proteolytic activity of CTSD causes the severe neurodegenerative disorder NCL type 10 leading to death of patients within hours after birth [6,7]. In our study, we investigated the impact of CTSD inhibition on protein turnover during neuronal differentiation. The human LUHMES cell line was used as model for the differentiation of neuronal precursor cells into dopaminergic neurons [15]. To model CTSD deficiency at selected stages of the process, we treated LUHMES cells during defined time periods of neuronal differentiation (Figs. 1A–3A and 5A) with Pepstatin A, an inhibitor of aspartic proteases active in the acidic milieu.

On the level of cell phenotype, the experiments demonstrated an accumulation of vesicles originating from the acidic

compartment, such as lysosomes, especially in late stages of differentiation. Likewise, we found stabilization of multiple proteins belonging to lysosomes as well as to the vesicular system including the endoplasmic reticulum (ER) and Golgi apparatus in the protein turnover experiments performed during late neuronal differentiation. High LAMP1 levels, a lysosomal membrane protein, were also verified in Pepstatin A-treated mature LUHMES cells (d6) as well as a whole brain lysate of a *Ctsd*-deficient mouse compared to controls. Importantly, NCL type 10 patients harboring mutations that impair the catalytic activity of CTSD show the same principal clinical symptoms as patients with mutations that abolish the expression of CTSD [2,3,7]. Thus, inhibition of CTSD by Pepstatin A seems to be sufficient to recapitulate a loss of CTSD activity as well as total protein expression as evident in patients with NCL type 10. This validates the suitability of LUHMES cells as a human *in vitro* model to investigate how inhibition of CTSD affects protein turnover in cells undergoing neuronal differentiation.

Interestingly, overall protein turnover is identical comparing Pepstatin A treatment with the solvent (DMSO) treated control condition during both early and late neuronal differentiation. A similar phenotype was previously shown in fibroblasts derived from constitutive *Ctsd*-deficient or control mice [12]. In this paper, the release of [³⁵S]methionine from metabolically labelled cellular proteins showed no difference between *Ctsd* knock-out and treatment of wildtype cells with Pepstatin A for up to 6 days. These results indicate that lysosomal bulk proteolysis is not affected by CTSD inhibition or CTSD deficiency in a human or murine *in vitro* model, respectively. Further, it has been reported that lysosomal protease deficiency can cause a STAT3-dependent induction of other lysosomal proteases and other hydrolases, which compensates the initial impairment of lysosomal proteolytic capacity [32]. For example, quiescent *Ctsd*^{−/−} breast cancer cells upregulate cathepsin L and are able to produce high levels of essential amino acids derived from proteolysis [16]. Therefore, we hypothesized that CTSD deficiency dysregulates the stability of certain individual proteins.

Notably, a previous proteomic study analyzed synaptosomes isolated from the cerebrum of three *Ctsd*^{−/−} mice at postnatal day 24 using shotgun proteomics [33]. This analysis of the steady state of these synapses revealed differential expression levels of proteins belonging to the energy metabolism, cytoskeleton, vesicular transport system, mitogen-activated protein kinase (MAPK) and transforming growth factor β (TGFβ) signaling upon CTSD deficiency. Interestingly, similar clusters like mitochondria (energy metabolism), cytoskeleton and vesicular (transport) system came also up in our pulse-chase SILAC experiment for early and/or late neuronal differentiation. However, with our approach we were able to analyze dynamic changes of protein stability within these clusters during different stages of neuronal differentiation and gained insights into the complexity of disease development.

In our study, we observed more than 70 proteins being stabilized or destabilized upon Pepstatin A treatment during early as well as late neuronal differentiation. STRING analysis revealed that especially mitochondrial proteins seem to be affected by CTSD inhibition. During early differentiation, Pepstatin A treatment enhanced the stability of proteins belonging to the electron transport chain. However, this class of proteins together with proteins of the tricarboxylic acid cycle (TCA) are destabilized during late differentiation, while proteins important for fatty acid oxidation are

Fig. 4. Protein stability in LUHMES cells treated with Pepstatin A during early neuronal differentiation. (A) Heat map of protein stability in LUHMES cells upon Pepstatin A treatment at 0 h, 12 h, 24 h, and 48 h after switch to heavy label during early neuronal differentiation. (B) Change of protein stability in LUHMES cells upon Pepstatin A treatment averaged over 12 h, 24 h and 48 h after switch to heavy label during early neuronal differentiation. Classification into stabilized proteins (red) and destabilized proteins (blue) being higher or lower than $\pm 1 \times$ standard deviation (SD), respectively. (C) Clusters from STRING analysis during early neuronal differentiation with stabilized and destabilized proteins in LUHMES cells upon Pepstatin A treatment averaged over 12 h, 24 h and 48 h after label switch. (n = 3 independent experiments).

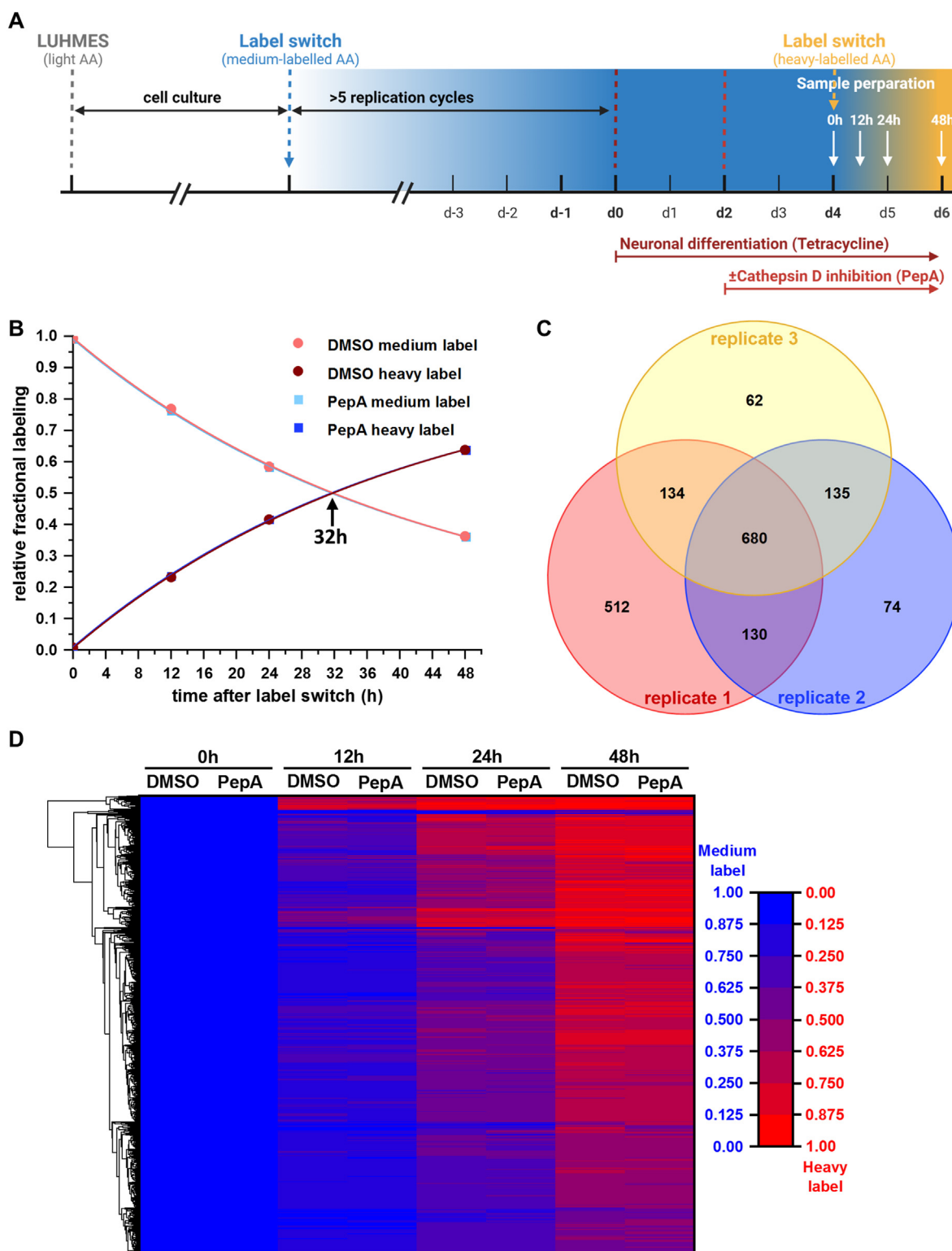
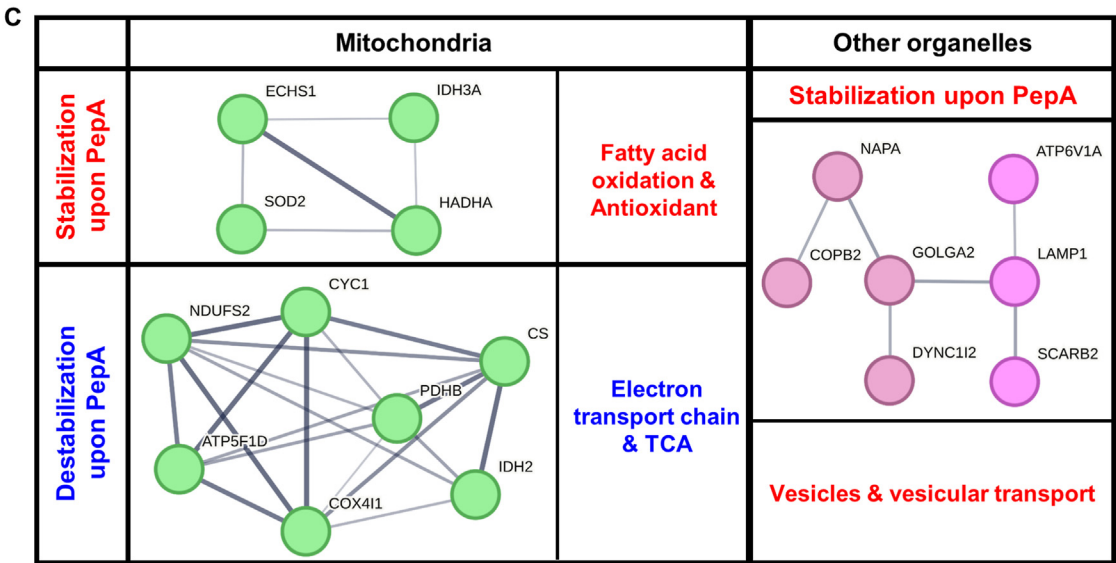
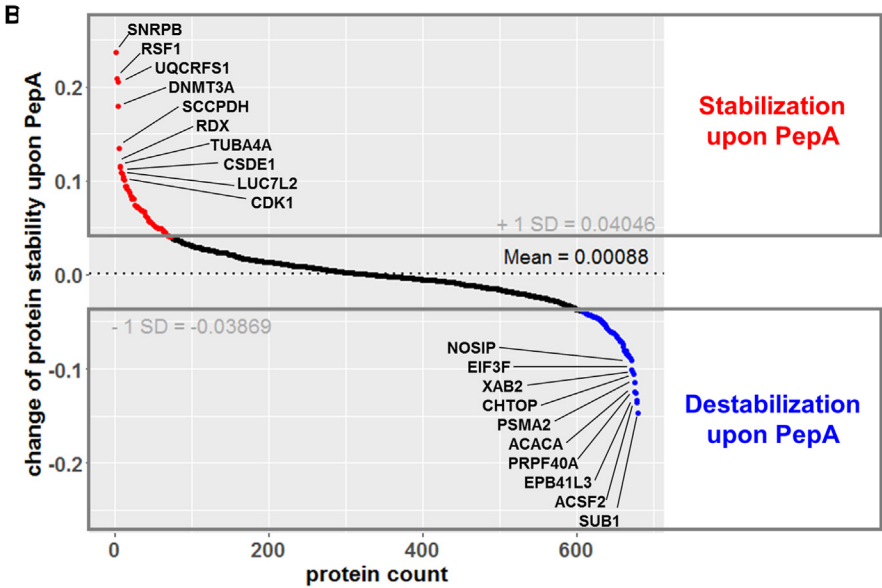
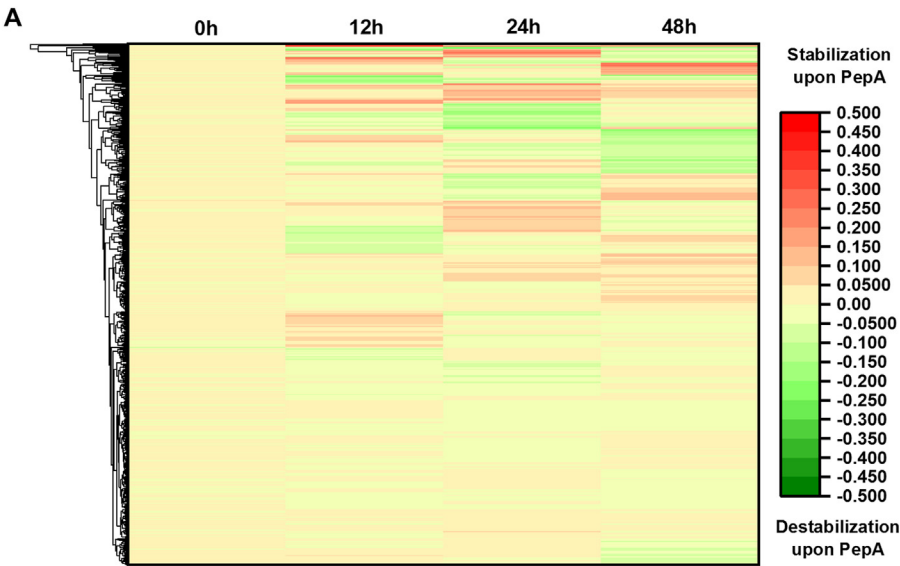


Fig. 5. Protein turnover in LUHMES cells treated with Pepstatin A during late neuronal differentiation. (A) Outline of neuronal differentiation of LUHMES cells, treatment with 15 μ M Pepstatin A and label switches (created with [BioRender.com](#)). (B) Change of relative fractional labelling for medium (light red: DMSO; light blue: PepA) and heavy label (dark red: DMSO; dark blue: PepA) in LUHMES cells \pm 15 μ M Pepstatin A at 0 h, 12 h, 24 h and 48 h after switch to heavy label during late neuronal differentiation. (C) Venn diagram showing detected proteins in three independent biological replicates of LUHMES cells used for SILAC experiment during late neuronal differentiation. (D) Heat map of protein decay in LUHMES cells \pm 15 μ M Pepstatin A at 0 h, 12 h, 24 h, and 48 h after switch to heavy label during late neuronal differentiation. (n = 3 independent experiments).



stabilized. This tendency was verified on protein level by analyzing three mitochondrial proteins, which were stabilized or destabilized upon Pepstatin A treatment in this SILAC turnover study. How does CTSD exert this regulation of energy production in mitochondria?

Lysosomes are not only important degradation machineries for proteins but also for organelles like mitochondria [34]. In this process called mitophagy, dysfunctional mitochondria are engulfed by autophagosomes, which fuse with lysosomes and are thus degraded. In an *in vitro* model of Alzheimers disease, reduced mitophagy was accompanied by low mitochondrial energy production and a loss of synaptic protrusions [35]. Enhancing mitophagy restored the energetic status of diseased neurons, demonstrating that mitophagy removes dysfunctional mitochondria to maintain a pool of functional mitochondria. However, no proteins contributing to mitophagy were identified in our SILAC approach. Nevertheless, the stabilization of proteins involved in the electron transport chain upon Pepstatin A treatment during early neuronal differentiation in our study may represent the accumulation of dysfunctional mitochondria and/or a compensatory mechanism to overcome the metabolic deficit due to defective mitophagy.

In general, the electron transport chain rather than fatty acid oxidation produces most of the energy used by neurons [36], because neurons have a limited capacity to deal with cytotoxic reactive oxygen species (ROS) generated by all pathways for cellular respiration [37]. Surprisingly, CTSD-inhibited LUHMES cells stabilize proteins involved in fatty acid oxidation during late neuronal differentiation, which may compensate and provide more sources for the limited energy produced by electron transport chain during early neuronal differentiation. In line with this, superoxide dismutase 2 (SOD2) is also stabilized to clear the neurons from ROS indicating higher levels of these harmful molecules due to dysregulated mitochondrial energy production [38]. A study in HeLa cells demonstrated that ROS production is also accelerated by CTSD knockdown due to leakage of iron from dysfunctional lysosomes into the cytosol, which may contribute to the stabilization of SOD2 in our system [39].

Interestingly, mitochondrial function seems to be important for the neuronal differentiation process. A study revealed that neuroblast cells with dysfunctional mitochondria showed an impairment of neuronal differentiation [36]. These cells upregulate fatty acid oxidation due to a limited energy supply, which seems to favor a proliferative cell state of the neuroblast cells. Our result suggest a similar mechanism, because during early neuronal differentiation, many proteins involved in neurite and axonal outgrowth, which is part of the neuronal differentiation process, were stabilized upon Pepstatin A treatment. However, during late differentiation, when CTSD-inhibited LUHMES cells switched to fatty acid oxidation, this cluster disappeared from the STRING analysis. These results demonstrate the complexity and connection of various pathways leading to the phenotype observed *in vitro* and *in vivo*.

Another important pathway identified to be differentially stabilized upon Pepstatin A treatment only during late neuronal differentiation was the UPS. Here, the deubiquitinating enzyme USP7 was stabilized due to Pepstatin A reducing the pool of potential proteins for proteasomal degradation [28]. In contrast, PSMA2 responsible for proteolytic cleavage of proteins in the 26S proteasome [29] as well as TPP2 cleaving tripeptides from N-termini of already processed proteins leaving the proteasome [30] were

destabilized in our experiments. Since UPS and autophagy facilitating lysosomes for protein degradation are the two major pathways to degrade proteins in a cell, one would expect that they compensate for each other in case of failure of one of the pathways [40]. However, the regulation seems to be more complex and it was shown that impairment of autophagy as expected by inhibiting a major lysosomal hydrolase like CTSD as in our experiments can have either activating or inhibiting effects on the proteasome dependent on the defect in autophagy. In our experiments, inhibition of CTSD by Pepstatin A seems to reduce the activity of the proteasome, which may also contribute to the stabilization of some of the identified proteins and therefore, be only indirectly mediated by the lysosomal dysfunction.

5. Conclusion

Taken together, our results demonstrate that the LUHMES cell line in combination with Pepstatin A treatment to inhibit CTSD activity is a suitable model to study NCL type 10 *in vitro*. Notably, Pepstatin A treatment did not change lysosomal bulk proteolysis neither during early nor late neuronal differentiation. Instead, individual proteins belonging to different compartments and pathways in the cell were dysregulated upon Pepstatin A treatment. The most prominent change was observed for mitochondrial proteins indicating a failure of energy production in CTSD-inhibited cells. Therefore, we hypothesize that mitochondrial dysfunction upon CTSD inhibition is a driving force for the successive loss of neurons in CTSD-deficient mice and patients with NCL type 10.

Funding

This work was supported by the Deutsche Forschungsgemeinschaft (DFG), under Germany's Excellence Strategy (BIOSS-EXC-294), GRK2606 (Project ID 423813989; to T.R. and O.S.) and the German Cancer Consortium DKTK (FR01-371 T.R.). O.S. acknowledges further funding by the Deutsche Forschungsgemeinschaft (DFG, projects 446058856, 466359513, 444936968, 405351425, 431336276, 43198400 (SFB 1453 "Neph-Gen"), 441891347 (SFB 1479 "OncoEscape"), 322977937 (GRK 2344 "MeInBio"), the ERA PerMed program (BMBF, 01KU1916, 01KU1915A), the German Consortium for Translational Cancer Research (project Impro-Rec), the MatrixCode research group, FRIAS, Freiburg, the investBW program BW1_1198/03, and the ERA TransCan program (projects 01KT2201, "PREDICO" and 01KT2333, "ICC-Strat").

Author contributions

Conceptualization, J.S. and T.R.; methodology, J.S., D.V., M.H. and T.R.; data curation, J.S., L.H., D.V., O.S. and T.R.; writing-original draft preparation, L.H. and T.R.; writing-review and editing, L.H. and T.R.; visualization, J.S., L.H. and T.R.; supervision, J.M. and T.R.; project administration, T.R.; funding acquisition, O.S. and T.R. All authors have read and agreed to the published version of the manuscript.

Data availability

The data generated in this study are available within the article, its supplementary data files and upon request by contact with the

Fig. 6. Protein stability in LUHMES cells treated with Pepstatin A during late neuronal differentiation. (A) Heat map of protein stability in LUHMES cells upon Pepstatin A treatment at 0 h, 12 h, 24 h, and 48 h after switch to heavy label during late neuronal differentiation. (B) Change of protein stability in LUHMES cells upon Pepstatin A treatment averaged over 12 h, 24 h and 48 h after switch to heavy label during late neuronal differentiation. Classification into stabilized proteins (red) and destabilized proteins (blue) being higher or lower than $\pm 1\times$ standard deviation (SD), respectively. (C) Clusters from STRING analysis during late neuronal differentiation with stabilized and destabilized proteins in LUHMES cells upon Pepstatin A treatment averaged over 12 h, 24 h and 48 h after label switch. (n = 3 independent experiments).

corresponding author.

Declaration of competing interest

The authors declare that they have no conflict of interest.

Acknowledgements

The authors thank Susanne Dollwet-Mack (Institute for Molecular Medicine and Cell Research Freiburg, Germany) for her technical assistance and Marcel Leist (University of Konstanz, Germany) for providing the LUHMES cell line.

Appendix A. Supplementary data

Supplementary data to this article can be found online at <https://doi.org/10.1016/j.biochi.2024.03.013>.

References

- [1] C.C. Tan, J.T. Yu, M.S. Tan, T. Jiang, X.C. Zhu, L. Tan, Autophagy in aging and neurodegenerative diseases: implications for pathogenesis and therapy, *Neurobiol. Aging* 35 (2014) 941–957, <https://doi.org/10.1016/j.neurobiolaging.2013.11.019>.
- [2] S. Ketterer, A. Gomez-Auli, L.E. Hillebrand, A. Petrer, A. Ketscher, T. Reinheckel, Inherited diseases caused by mutations in cathepsin protease genes, *FEBS J.* 284 (2017) 1437–1454, <https://doi.org/10.1111/febs.13980>.
- [3] E. Seranova, K.J. Connolly, M. Zatyka, T.R. Rosenstock, T. Barrett, R.I. Tuxworth, S. Sarkar, Dysregulation of autophagy as a common mechanism in lysosomal storage diseases, *Essays Biochem.* 61 (2017) 733–749, <https://doi.org/10.1042/EBC20170055>.
- [4] S.E. Mole, S.L. Cotman, Genetics of the neuronal ceroid lipofuscinoses (Batten disease), *Biochim. Biophys. Acta, Mol. Basis Dis.* 1852 (2015) 2237–2241, <https://doi.org/10.1016/j.bbadis.2015.05.011>.
- [5] R.E. Williams, S.E. Mole, New nomenclature and classification scheme for the neuronal ceroid lipofuscinoses, *Neurology* 79 (2012) 183–191, <https://doi.org/10.1212/WNL.0b013e31825f0547>.
- [6] E. Siintola, S. Partanen, P. Strömme, A. Haapanen, M. Haltia, J. Maehlen, A.E. Lehesjoki, J. Tynnelä, Cathepsin D deficiency underlies congenital human neuronal ceroid-lipofuscinosis, *Brain* 129 (2006) 1438–1445, <https://doi.org/10.1093/brain/awl107>.
- [7] R. Steinfeld, K. Reinhardt, K. Schreiber, M. Hillebrand, R. Kraetzner, W. Brück, P. Saftig, J. Gärtner, Cathepsin D deficiency is associated with a human neurodegenerative disorder, *Am. J. Hum. Genet.* 78 (2006) 988–998, <https://doi.org/10.1086/504159>.
- [8] P.L. Faust, S. Kornfeld, J.M. Chirgwin, Cloning and sequence analysis of cDNA for human cathepsin D, *Proc. Natl. Acad. Sci. U. S. A.* 82 (1985) 4910–4914, <https://doi.org/10.1073/pnas.82.15.4910>.
- [9] M. Koike, H. Nakanishi, P. Saftig, J. Ezaki, K. Isahara, Y. Ohsawa, W. Schulz-Schaeffer, T. Watanabe, S. Waguri, S. Kametaka, M. Shibata, K. Yamamoto, E. Kominami, C. Peters, K. Von Figura, Y. Uchiyama, Cathepsin D deficiency induces lysosomal storage with ceroid lipofuscin in mouse CNS neurons, *J. Neurosci.* 20 (2000) 6898–6906, <https://doi.org/10.1523/JNEUROSCI.20-18-06898.2000>.
- [10] R. Yamasaki, J. Zhang, I. Koshiishi, D.F. Sastradipura Suniarti, Z. Wu, C. Peters, M. Schwake, Y. Uchiyama, J. ichi Kira, P. Saftig, H. Utsumi, H. Nakanishi, Involvement of lysosomal storage-induced p38 MAP kinase activation in the overproduction of nitric oxide by microglia in cathepsin D-deficient mice, *Mol. Cell. Neurosci.* 35 (2007) 573–584, <https://doi.org/10.1016/j.mcn.2007.05.002>.
- [11] A. Ketscher, S. Ketterer, S. Dollwet-Mack, U. Reif, T. Reinheckel, Neuroectoderm-specific deletion of cathepsin D in mice models human inherited neuronal ceroid lipofuscinosis type 10, *Biochimie* 122 (2016) 219–226, <https://doi.org/10.1016/j.biochi.2015.07.020>.
- [12] P. Saftig, M. Hetman, W. Schmahl, K. Weber, L. Heine, H. Mossmann, A. Köster, B. Hess, M. Evers, K. Von Figura, C. Peters, Mice deficient for the lysosomal proteinase cathepsin D exhibit progressive atrophy of the intestinal mucosa and profound destruction of lymphoid cells, *EMBO J.* 14 (1995) 3599–3608, <https://doi.org/10.1002/j.1460-2075.1995.tb00029.x>.
- [13] A.R.A. Marques, A. Di Spiezo, N. Thießen, L. Schmidt, J. Grötzinger, R. Lüllmann-Rauch, M. Damme, S.E. Storck, C.U. Pietrzik, J. Fogh, J. Bär, M. Mikhaylova, M. Glatzel, M. Bassal, U. Bartsch, P. Saftig, Enzyme replacement therapy with recombinant pro-CTSD (cathepsin D) corrects defective proteolysis and autophagy in neuronal ceroid lipofuscinosis, *Autophagy* 16 (2020) 811–825, <https://doi.org/10.1080/15548627.2019.1637200>.
- [14] A. Schulz, T. Ajayi, N. Specchio, E. de Los Reyes, P. Gissen, D. Ballon, J.P. Dyke, H. Cahan, P. Slator, D. Jacoby, A. Kohlschütter, Study of intraventricular cerliponase alfa for CLN2 disease, *N. Engl. J. Med.* 378 (2018) 1898–1907, <https://doi.org/10.1056/NEJM0A1712649>.
- [15] D. Scholz, D. Pörtl, A. Genewsky, M. Weng, T. Waldmann, S. Schildknecht, M. Leist, Rapid, complete and large-scale generation of post-mitotic neurons from the human LUHMES cell line, *J. Neurochem.* 119 (2011) 957–971, <https://doi.org/10.1111/j.1471-4159.2011.07255.x>.
- [16] S. Ketterer, J. Mitschke, A. Ketscher, M. Schlimpert, W. Reichardt, N. Baeuerle, M.E. Hess, P. Metzger, M. Boerries, C. Peters, B. Kammerer, T. Brummer, F. Steinberg, T. Reinheckel, Cathepsin D deficiency in mammary epithelium transiently stalls breast cancer by interference with mTORC1 signaling, *Nat. Commun.* 11 (2020) 5133, <https://doi.org/10.1038/s41467-020-18935-2>.
- [17] A. Bettecken, L. Heß, L. Hölzen, T. Reinheckel, Dipeptidyl-aminopeptidases 8 and 9 regulate autophagy and tamoxifen response in breast cancer cells, *Cells* 12 (2023) 2031, <https://doi.org/10.3390/cells2162031>.
- [18] K. Fröhlich, E. Brombacher, M. Fahrner, D. Voge, L. Kook, N. Pinter, P. Bronsert, S. Timme-Bronsert, A. Schmidt, K. Bärenfaller, C. Kreutz, O. Schilling, Benchmarking of analysis strategies for data-independent acquisition proteomics using a large-scale dataset comprising inter-patient heterogeneity, *Nat. Commun.* 13 (2022) 2622, <https://doi.org/10.1038/s41467-022-30094-0>.
- [19] M. Hailemariam, R.V. Eguiz, H. Singh, S. Bekele, G. Ameni, R. Pieper, Y. Yu, S-trap, an ultrafast sample-preparation approach for shotgun proteomics, *J. Proteome Res.* 17 (2018) 2917–2924, <https://doi.org/10.1021/ACS.JPROTEOME.8B00505>.
- [20] A.T. Kong, F. V. Leprevost, D.M. Avtonomov, D. Mellacheruvu, A.I. Nesvizhskii, MSFragger: ultrafast and comprehensive peptide identification in shotgun proteomics, *Nat. Methods* 14 (2017) 513–520, <https://doi.org/10.1038/nmeth.4256>.
- [21] F. Da, V. Leprevost, S.E. Haynes, D.M. Avtonomov, H.-Y. Chang, A.K. Shanmugam, D. Mellacheruvu, A.T. Kong, A.I. Nesvizhskii, Philosopher: a versatile toolkit for shotgun proteomics data analysis, *Nat. Methods* 17 (2020) 869–870, <https://doi.org/10.5281/zenodo.3909842>.
- [22] F. Yu, S.E. Haynes, A.I. Nesvizhskii, IonQuant enables accurate and sensitive label-free quantification with FDR-controlled match-between-runs, *Mol. Cell. Proteomics* 20 (2021) 100077, <https://doi.org/10.1016/j.mcpro.2021.100077>.
- [23] H. Wickham, M. Averick, J. Bryan, W. Chang, L. McGowan, R. François, G. Grolemund, A. Hayes, L. Henry, J. Hester, M. Kuhn, T. Pedersen, E. Miller, S. Bache, K. Müller, J. Ooms, D. Robinson, D. Seidel, V. Spinu, K. Takahashi, D. Vaughan, K. Wilke, K. Woo, H. Yutani, Welcome to the tidyverse, *J. Open Source Softw.* 4 (2019) 1686, <https://doi.org/10.21105/joss.01686>.
- [24] D. Szklarczyk, A.L. Gable, D. Lyon, A. Junge, S. Wyder, J. Huerta-Cepas, M. Simonovic, N.T. Doncheva, J.H. Morris, L.J. Jensen, C. Von Mering, STRING v11: protein-protein association networks with increased coverage, supporting functional discovery in genome-wide experimental datasets, *Nucleic Acids Res.* 47 (2018) 607–613, <https://doi.org/10.1093/nar/gky1131>.
- [25] M. Hoshimaru, J. Ray, D.W. Sah, F.H. Gage, Differentiation of the immortalized adult neuronal progenitor cell line C2C12 into neurons by regulatable suppression of the v-myc oncogene, *Proc. Natl. Acad. Sci. USA* 93 (1996) 1518–1523, <https://doi.org/10.1073/pnas.93.4.1518>.
- [26] M. Uhlen, C. Zhang, S. Lee, E. Sjöstedt, L. Fagerlitz, G. Bidkhor, R. Benfeitas, M. Arif, Z. Liu, F. Edfors, K. Sanli, K. Von Feilitzen, P. Oksvold, E. Lundberg, S. Hober, P. Nilsson, J. Mattsson, J.M. Schwenk, H. Brunnström, B. Glimelius, T. Sjöblom, P.H. Edqvist, D. Djureinovic, P. Mücke, C. Lindskog, A. Mardinoglu, F. Ponten, A pathology atlas of the human cancer transcriptome, *Science* 1979 (2017) 357, <https://doi.org/10.1126/SCIENCE.AAN2507>.
- [27] C. Compagnucci, F. Piemonte, A. Sferri, E. Piermarini, E. Bertini, The cytoskeletal arrangements necessary to neurogenesis, *Oncotarget* 7 (2016) 19414–19429, <https://doi.org/10.18632/oncotarget.6838>.
- [28] A. Pozhidaeva, I. Bezsonova, USP7: structure, substrate specificity, and inhibition, *DNA Repair* 76 (2019) 30–39, <https://doi.org/10.1016/j.dnarep.2019.02.005>.
- [29] M.-U. Rashid, S. Lorzadeh, A. Gao, S. Ghavami, K.M. Coombs, PSMA2 knock-down impacts expression of proteins involved in immune and cellular stress responses in human lung cells, *Biochem. Biophys. Acta Mol. Basis Dis.* 1869 (2022) 166617, <https://doi.org/10.1016/j.bbadis.2022.166617>.
- [30] E.M. Reinthaler, E. Graf, T. Zrzavy, T. Wieland, C. Hotzy, C. Kopecky, S. Pferschy, C. Schmied, F. Leutmezer, M. Keilani, C.M. Lill, S. Hoffjan, J.T. Epplen, U.K. Zettl, M. Hecker, A. Deutschländer, S.G. Meuth, M. Ahrm, B. Mustafa, M. El-Khateeb, C. Vilariño-Güell, A. Dossa Sadovnick, F. Zimprich, B. Tomkinson, T. Strom, W. Kristoferitsch, H. Lassmann, A. Zimprich, TPP2 mutation associated with sterile brain inflammation mimicking MS, *Neurol. Genet.* 4 (2018) e285, <https://doi.org/10.1212/NXG.0000000000000285>.
- [31] C. Oberle, J. Huai, T. Reinheckel, M. Tacke, M. Rassner, P.G. Ekert, J. Buellesbach, C. Borner, Lysosomal membrane permeabilization and cathepsin release is a Bax/Bak-dependent, amplifying event of apoptosis in fibroblasts and monocytes, *Cell Death Differ.* 17 (2010) 1167–1178, <https://doi.org/10.1038/cdd.2009.214>.
- [32] J. Martínez-Fábregas, A. Prescott, S. Van Kasteren, D.L. Pedrioli, I. Mclean, A. Moles, T. Reinheckel, V. Poli, C. Watts, Lysosomal protease deficiency or substrate overload induces an oxidative-stress mediated STAT3-dependent pathway of lysosomal homeostasis, *Nat. Commun.* 9 (2018) 5343, <https://doi.org/10.1038/s41467-018-07741-6>.
- [33] S. Koch, E. Scifo, A. Rokka, P. Trippner, M. Lindfors, R. Korhonen, G.L. Corthals, I. Virtanen, M. Lalowski, J. Tynnelä, Cathepsin D deficiency induces cytoskeletal changes and affects cell migration pathways in the brain, *Neurobiol. Dis.* 50 (2012) 107–119, <https://doi.org/10.1016/j.nbd.2012.10.004>.
- [34] N. Mizushima, M. Komatsu, Autophagy: renovation of cells and tissues, *Cell*

- 147 (2011) 728–741, <https://doi.org/10.1016/j.cell.2011.10.026>.
- [35] S. Han, M. Zhang, Y.Y. Jeong, D.J. Margolis, Q. Cai, The role of mitophagy in the regulation of mitochondrial energetic status in neurons, *Autophagy* 17 (2021) 4182–4201, <https://doi.org/10.1080/15548627.2021.1907167>.
- [36] M. Audano, S. Pedretti, M. Crestani, D. Caruso, E. De Fabiani, N. Mitro, Mitochondrial dysfunction increases fatty acid β -oxidation and translates into impaired neuroblast maturation, *FEBS Lett.* 593 (2019) 3173–3189, <https://doi.org/10.1002/1873-3468.13584>.
- [37] P.S. Baxter, G.E. Hardingham, Adaptive regulation of the brain's antioxidant defences by neurons and astrocytes, *Free Radic. Biol. Med.* 100 (2016) 147–152, <https://doi.org/10.1016/j.freeradbiomed.2016.06.027>.
- [38] C. Quijano, M. Trujillo, L. Castro, A. Trostchansky, Interplay between oxidant species and energy metabolism, *Redox Biol.* 8 (2016) 28–42, <https://doi.org/10.1016/j.redox.2015.11.010>.
- [39] S. Su, X. Zhu, L. Lin, X. Chen, Y. Wang, J. Zi, Y. Dong, Y. Xie, Y. Zhu, J. Zhang, J. Zhu, D. Xu, N. Xu, X. Lou, S. Liu, Lowering endogenous cathepsin D abundance results in reactive oxygen species accumulation and cell senescence, *Mol. Cell. Proteomics* 16 (2017) 1217–1232, <https://doi.org/10.1074/mcp.M115.050179>.
- [40] Y. Li, S. Li, H. Wu, Ubiquitination-proteasome system (UPS) and autophagy two main protein degradation machineries in response to cell stress, *Cells* 11 (2022) 851, <https://doi.org/10.3390/cells11050851>.